WARSAW UNIVERSITY OF TECHNOLOGY Index 351733
FACULTY OF CIVIL ENGINEERING
COMMITTEE FOR CIVIL AND WATER ENGINEERING
POLISH ACADEMY OF SCIENCES ISSN 1230-2945

DOI: 10.24425/ace.2023.147662

ARCHIVES OF CIVIL ENGINEERING

Vol. LXIX ISSUE 4 2023

pp. 319 –337

Research paper

Experimental study of a new type of high-strength monolithic square-section concrete columns with spiral stirrups

Zheng Xianchao[1], Fan Liyun[2], Jun Zhao[3]

Abstract: In this paper, four full-scale concrete columns with high-strength spiral stirrups (HSSS) are constructed and tested under low-cycle repeated loading. The specimens consisted of two cast-in-place columns and two precast concrete columns encased by a partly square steel pipe and bolt bars.The structural analysis of the HSSS columns of precast concrete conducted here is novel, and past experimental data for this are not available.To assess the seismic behavior and failure mechanisms of the new connections, quasi-static tests were carried out on columns prefabricated with them and cast-in-place specimens.The responses of all columns were compared, and the results showed that the failure modes of all columns are the large eccentric damage, and the destruction of all specimens occur at the column foot. The anti-seismic property of the precast HSSS concrete columns was comparable to that of the HSSS cast-in-place columns. A comparison of such performance parameters as energy dissipation and coefficient of ductility revealed that the precast HSSS concrete columns are suitable for use in earthquake zones.

Keywords: square steel pipe and bolt bars (SSPBB), hysteresis analysis, high-strength spiral stirrups (HSSS), low-cycle repeated loading

[1]Associate Prof., PhD., Eng., Department of Civil and Architecture Engineering in Hezhou University, Hezhou 542899, China, e-mail: zhxch603@126.com, ORCID: 0000-0003-3924-2309

[2]MSc., Eng., Department of Civil and Architecture Engineering in Hezhou University, Hezhou 542899, China, e-mail: fly_fanliyun@163.com, ORCID: 0009-0004-9104-6967

[3]Associate Prof.,Department of Civil and Architectural Engineering in Anyang Institute of Technology, Anyang, Henan Province, 455000, China, e-mail: 20160428@ayit.edu.cn, ORCID: 0000-0002-1933-9851

1. Introduction

The structure-destructive testing and collapse mechanisms of buildings show that the deformation capacity of frame columns is a major factor influencing the performance of frameworks designed to resist major earthquakes [1]. For HSSS columns, the boundary between large and small eccentric compressions ranges from 0.35 to 1.0 or higher, which improves the ductility of concrete columns with high-strength spiral stirrups [2]. The problem of controlling section size using the axial compression ratio can thus be solved. An experimental study of the behaviour of the concrete columns confined by helical reinforcement of 500 MPa and with 500 MPa longitudinal reinforcement has been presented. With this variation in design, a higher strength, yet more ductile column can be achieved [3]. Based on the test results of concrete columns confined by high-strength stirrups under lateral cyclic loading, it is found that stirrup yield strength could not be used directly in calculating bearing capacity, because the high-strength stirrup could not yield at the peak point. The concrete columns confined by high-strength stirrups exhibited higher bearing capacity and better deformation ability [4, 5].

The use of HSSS columns in current architectural designs has been limited to cast-in-place columns. Precast concrete provides high-quality structural elements, construction efficiency, and savings in terms of time and cost of investment [6]. The performance and capacity of specially designed connections have been evaluated to validate these benefits and help expand the market for precast concrete structures in seismic zones [7].

By use of the comparable full scale model test method, two confined concrete columns with horizontal strengthened bars spliced by grout sleeves and two cast-in site column with plain stirrups were designed and constructed. Through reversed low cyclic loading test, compared with the cast-in site column with plain stirrups, the bearing capacity and the seismic performance of the confined concrete column with horizontal bar was studied. This connection type is reliable [8]. A connections between precast concrete column and foundation can be achieved by inserting the extended longitudinal reinforcement in precast concrete column into the corrugated pipe with high-strength filler. The low-frequency cyclic loading test was conducted for eight precast concrete columns and one integral cast-in-place column for comparison [9]. Two prefabricated structural columns with slurry anchor lapping of corrugated pipe restrained by spiral stirrup were designed and manufactured. The quasi-static load test was carried out to analyze the failure mode, hysteretic curve, skeleton curve, bearing capacity, ductility, stiffness degradation curve and energy dissipation capacity of the structural columns [10].

A column–column dry connection of a prefabricated concrete frame structure was reported by China College of Civil Engineering in Southeast University [11]. Welding was the basic technique used for this type of connection. The method of connection is one where the vertical load transfers through concrete, whereas shear transfers through the stirrup and concrete cogging. The transfer paths of the forces become clearer as paths of shear and the bending moment are separated. Many precast concrete structures have been heavily damaged by recent earthquakes, and the poor performance of their connections might have been the primary reason for this [12, 13]. It is useful to investigate the reaction to earthquakes of pre-

fabricated columns with HSSS to determine whether they can provide satisfactory support in comparison with the cast-in-place specimens. A research program concerning the performance of column–column connections of precast concrete was pursued in China's Xi'an University of Arch. and Tech. A new type of column-to-column connection with a square steel pipe and bolt bar (SSPBB) has also been reported. Two HSSS columns were connected using a square steel pipe, and the gap between the pipe and the columns was filled with grout. To ensure the reliability of the connection of the prefabricated column, transverse reinforcement passes through the prefabricated column, and the reinforcement and steel pipe are welded together. The integrity of the prefabricated columns is not less than that of the cast-in-place columns–the so-called "square steel pipe and bolt bars column joint" (SSPBB). The prefabricated HSSS columns with SSPBB connection are shown in Fig. 1. This program was funded by China's Hebei Hechuang Building Technology Material Co. Ltd.

Fig. 1. SSPBB connection in practical project

2. Research significance

To assess the seismic behavior and failure mechanisms of the new connections, quasi-static tests were carried out on columns prefabricated with them and cast-in-place specimens. The test results can provide a better understanding of the shear capacity and hysteretic behavior of the prefabricated columns. Moreover, they can be used to validate whether the desired failure modes occur when they are designed according to building codes for full-scale connection specimens. All test specimens in this research program are detailed according to the governing building codes or the available literature [14].

3. Experimental procedure

The specimens in this test were two prefabricated columns and two cast-in-place comparison columns. The measurements (length, width and height) of all prefabricated columns were 400 mm×400 mm×1800 mm, and those of the foundations were 1400 mm×500 mm×

700 mm, as shown in Fig. 2. To research the anti-seismic property of the two prefabricated specimens, two cast HSSS concrete columns of the same size were made for comparison.

3.1. Design of specimens

Figs. 2 and 3 show details of the prefabricated specimens (Y01, Y02), and Fig. 4 shows the two cast columns (C01, C02). All the concrete columns with the HSSS contained eight main bars (HRB335) 22 mm in diameter arranged symmetrically along the perimeter. The horizontal bolt reinforcements of the prefabricated specimens (Y01, Y02) were composed of eight longitudinal bars (HRB335) of 20 mm in diameter each. The reinforced concrete columns with high-strength spiral reinforcement exhibited excellent behavior when subjected to loads. The HSSS in all columns consisted of four limbs steel wires (Φ^R) 5 mm in diameter, with a 50 mm spacing, as shown in Figs. 2 and 4. The yield strength of the high-strength reinforcement was over 1100 MPa. The thickness and the length of the steel pipe for the prefabricated columns (Y01, Y02) were 5 mm and 850 mm, respectively. To prevent the local yielding of the steel pipe, two 100 mm steel plates were welded on the

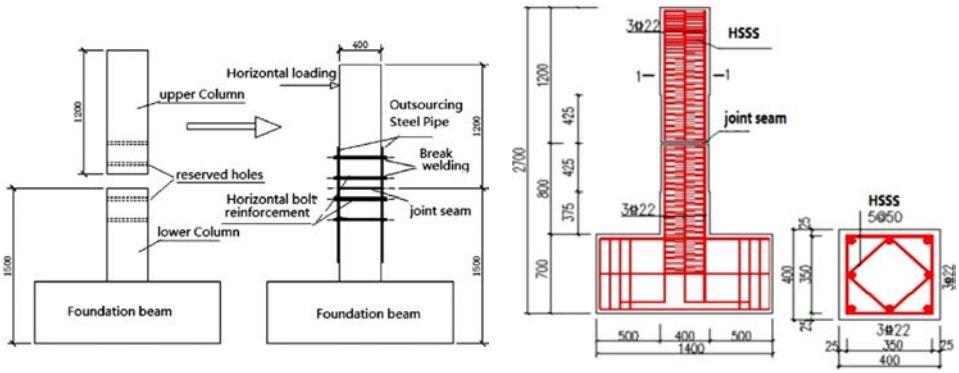

(a) (b)

Fig. 2. The size in mm of the prefabricated specimens Y01, Y02: (a) the assembly of columns, (b) the reinforcement of columns

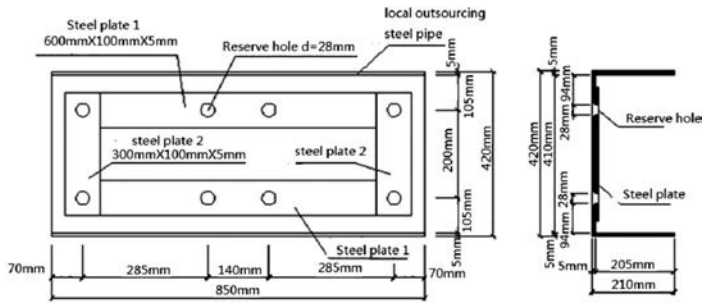

Fig. 3. Square steel pipe

east and west sides of the steel pipe. The joint between the two pre-sections was 800 mm from the bottom.

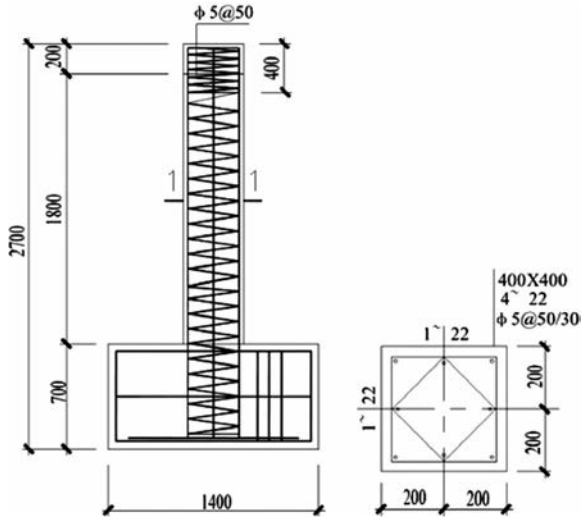

Fig. 4. The size in mm of the cast columns C01, C02

3.2. Materials

The test results for the steel and reinforcements materials are summarized in Table 1.The compressive strength (average) of the concrete cube at 28 days was 29.27 MPa. The concrete cube and all the concrete columns were cured for 28 days in a standard curing chamber, under a temperature of 20 ± 3°C, a relative humidity > 90% [15, 16].

Table 1. Material Properties (Yield Strength/Ultimate Strength)

Material, diameter (mm)	HRB335 Φ22	HRB335 Φ20	HPB235 Φ8	HSSS $\Phi^R 5$	Square steel pipe
Yielding strength (MPa)	360	360	290	1170	320
Tensile strength (MPa)	442.5	415	302.5	–	–

3.3. Experimental setup

The experiment was a pseudo-static test and the setup is shown in Fig. 5. Constant vertical load was applied by a vertical hydraulic actuator to the specimens by means of a link beam. Force transfer between the link beam and the top of the specimen was carried out by a roller bearing with negligible frictional force. Lateral load was applied by a horizontal hydraulic actuator with a maximum capacity of 2000 kN. The loading point

of the horizontal load was 1800 mm from the bottom of the column parallel to east/west. The actuator was connected to a rigid and strong reaction wall that transferred forces to the strong floor. The horizontal actuator was set to force–displacement mixed control mode and the vertical actuator was set to constant force control mode during the test. All actuators had built-in displacement meters and load cells connected to a digital control unit.

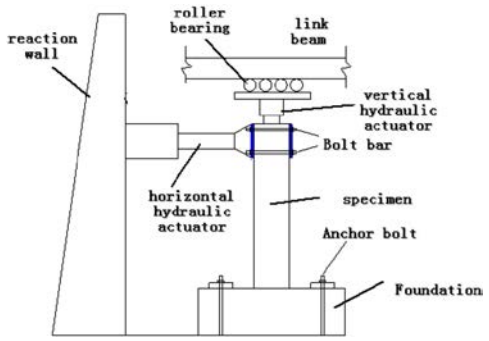

Fig. 5. Test setup

3.3.1. Instrumentation

Ten linear variable displacement transducers (LVDTs) were used for each specimen. An LVDT (S01) was installed to measure horizontal displacement on top of the specimen. Three LVDTs (S02, S03, and S04) were installed to measure rotation at three elevations: 100 mm, 200 mm and 300 mm, above the foundation on the east side of the specimen. Two LVDTs (S05, S06) were arranged to measure the bottom shear deformation of the column above the foundation on the north side of the specimen. Four other LVDTs (S07, S08, S09, and S10) were used to measure slip at the bottom and on top of the specimen. They were fixed to the concrete, and could measure movements of the square steel pipe. Figure 6 shows the arrangement of the LVDTs.

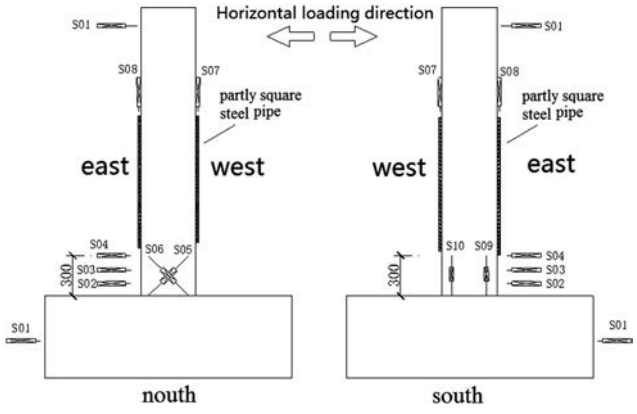

Fig. 6. Typical LVDTs arrangement on specimens

3.3.2. Test procedure

The force–displacement mixed loading process was used in tests as shown in Fig. 7. Displacement-controlled loading was used in the tests because it was not possible to study columnar behavior load capacity if a force-controlled loading scheme was used. Both yield load and yield displacement were calculated during the test. The process was as follows: When a small load was imposed on the specimens, the connections remained in an elastic state and the force–displacement relationships were linear. With the increase in applied load, an inflection point occurred and the force–displacement relationship changed to nonlinear. The rigidness of the specimen decreased at the point of inflection, and the corresponding load and displacement are referred to as the yield load and yield displacement, respectively. Three fully reversed cycles were applied at each drift ratio, and the drift ratios were set according to the yield displacement. This sequence was intended to ensure that the displacements increasing gradually in such steps were neither too large nor too small. The test was terminated before the specimen's bearing capacity dropped to below 85% of the ultimate bearing capacity [17, 18].

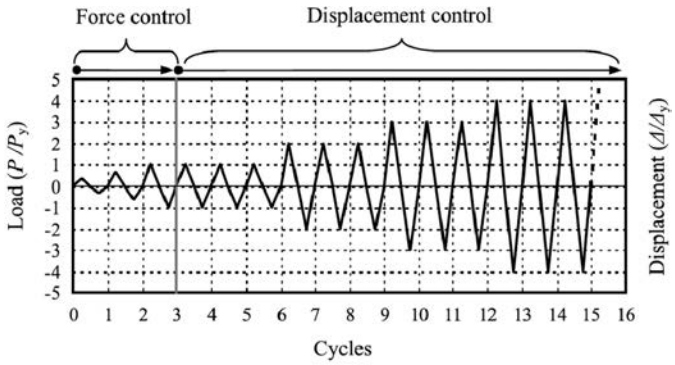

Fig. 7. Schematic view of loading history

3.3.3. The parameters of the experiment

The parameters of the experiment are shown in Table 2. The axial loads (N) were calculated by the axial pressure ratio (μ_n) and the concrete compressive strength (f_c) [19]. The ratios of reinforcement were calculated using Formula (3.2). The ratios ratios of shear span to effective depth (λ) were calculated using Formula (3.3). The volumetric ratio of the spiral reinforcement (ρ_v) was calculated using Formula (3.4).

$$N = \mu_n f_c b_c h_c \tag{3.1}$$

$$\rho_s = \frac{A_{sl}}{b_c h_c} \tag{3.2}$$

$$\lambda = l_n / h_c \tag{3.3}$$

where h_c is the depth of the concrete-assembled monolithic column; b_c is the thickness of the concrete column; A_{sl} is cross-section area of the eight main bars; l_n is the length of the

local outsourced steel tube.

$$\rho_v = \frac{A_s}{(D_c - d)s} \tag{3.4}$$

where A_s is cross-section area of spiral reinforcement; As shown in Fig. 8, D_c is diameter of core concrete; d is diameter of spiral spiral reinforcement; and s is pitch of spiral reinforcement which is the centerline-to-centerline distance between adjacent spiral reinforcement [19].

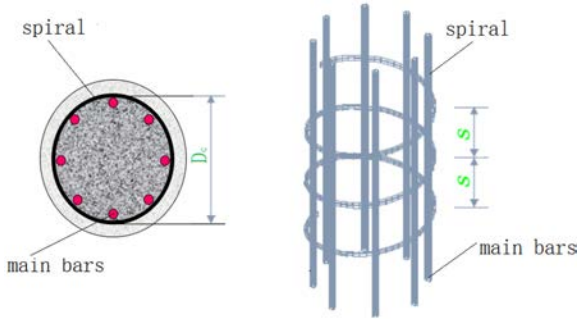

(a) (b)

Fig. 8. The spiral reinforcement

Table 2. Parameters of the specimens

Marks of the specimens	axial-pressure ratio μ_n	Ratio of reinforcement ρ_s	Ratio of shear span to effective depth λ	Volume ratio of spiral reinforcement	Axial pressure load N (kN)
C01	0.3	0.39%	4.5	0.79%	857.6
C02	1.0	0.39%	4.5	0.79%	2572.8
Y01	1.0	0.39%	4.5	0.79%	2572.8
Y02	0.3	0.39%	4.5	0.79%	857.6

4. Analytical procedure

4.1. Experimental observations of full-scale columns

Similar crack patterns were observed in all specimens up to a drift ratio of four times the yield displacement. Three concrete cracks developed at the three elevations. The first set of cracks were at the bottom of each column, whereas the second occurred at approximately

half the depth of the first cracks. The third set of cracks were at approximately the full depth of the first cracks. It is visually clear that the first cracks played a key role in the total deformations of the specimens. In the C02 and Y01 specimens (experimental axial pressure ratios were one), the first cracks were the most active, with larger openings. The third cracks were more active than the second cracks and had a trend of inclination, such as flexure shear cracks. In the C01 and Y02 (experimental axial pressure ratios were 0.3) specimens, the first cracks were similarly the most active, as in the C01 and Y02 specimens. However, the second cracks were more active than the third set of cracks, and exhibited a trend of inclination such as flexure cracks.

Fig. 9 shows the damaged specimens after the test. Damage was caused at the bottom of each column. Concrete at the bottom of each column was crushed and flaked off the column surface, and the stirrups were thus exposed as shown in Fig. 9. The test results show that flexural failure occurred in the destructive processes of both the cast-in-place columns and the prefabricated columns. The failure modes and responses under lateral loads for specimen C01 were similar to those of specimen Y02, whereas those of C02 were similar to Y02. During tests of specimens Y01 and Y02, the steel pipe, bolt reinforcement, and concrete at the joint did not yield, and slip between the steel pipe and the concrete column was not observed.

(a) (b) (c) (d)

Fig. 9. The damage of columns: (a) C01, 9b) C02, (c) Y01, (d) Y02

4.2. Evaluation of test results

In contrast to the experimental results of the two different axial-pressure ratio precast specimens with the cast ones, the anti-seismic property of these prefabricated specimens is not worse than the cast-in-place specimens. The following is the process of this contrast.

4.2.1. Specimen Y01 and C02

Fig. 10a shows the experimental responses of specimens Y01 and C02. The hysteretic response curve of Y01 was very similar to that of C02. The response curve of C02 was

approximately linear up to a displacement of 16.527 mm, and then entered the nonlinear phase. At a displacement of 37.19 mm, the curve gained its horizontal ultimate load of 298.8 kN, and then degrades with a constant slope of −2.75 kN/mm up to a displacement of 84.88 mm, where the loading gain was 167.5 kN. The response curve of Y01 was approximately linear up to a displacement of 14.578 mm, and then entered the nonlinear phase. At a displacement of 31.15 mm, the curve gained its horizontal ultimate load of 304.5 kN, and then degraded with a constant slope of 2.36 kN/mm up to a displacement of 97.08 mm where the loading gain was 149 kN. It is worth noting that in the loading phase of all specimens, the first cycle was similar to the second and third, but in the unloading phase, the first cycle was different from the second and third cycles. A comprehensive analysis of the hysteresis curve shows that those of Y01 and C02 were plump with slight pinching, which indicates that square steel pipe and bolt bar column joint was reliable. The two specimens were thus satisfactory in terms of ductility and energy dissipation.

In Fig. 10b, the backbone curves are plotted together. 1) The specimen's backbone curves are symmetric about the origin. 2) The backbone curves are divided clearly into the elastic stage, intensive stage, and strength degradation stage. 3) It is clear that the curves of C02 and Y01 began degrading at +40 mm on the positive, and at –40 mm and –30 mm on the negative sides, respectively. 4) The slope of degradation of the curve of Y01 is not smaller than that of C02.

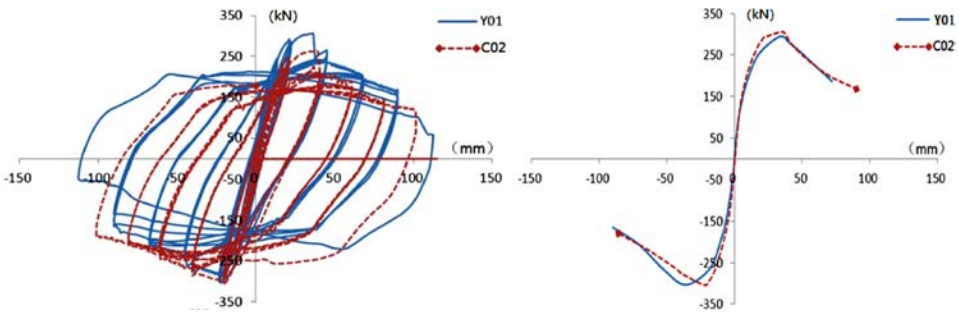

Fig. 10. Load-displacement response of C02 and Y01

All parameters pertaining to anti-seismic capability are summarized in Table 3. In Fig. 10b, the backbone curves are plotted together. 1) The specimen backbone curves are symmetric about the origin. 2) The backbone curves are divided clearly in the elastic stage, intensive stage and strength degradation stage. 3) It can be observed that the curves of C02 and Y01 degradation begin at +40 mm on the positive, while at –40 mm and –30 mm on the negative sides, respectively. 4) The curve degradation slope of the Y01 isn't less than C02. All the parameters of anti-seismic ability are summarized in Table 3.

The ultimate displacement (Δ_u) is the displacement which corresponds to 85% of the maximum force (p_u). It has been experimentally demonstrated and explained [20, 21] that the energy equivalent principle of the skeleton curve is used to determine the yield load (p_y) and yield displacement (Δ_y). The energy equivalent principle is shown at Fig. 11. The

Table 3. Parameters of anti-seismic ability of C02 and Y01

Marks of the specimen	Yield load (P_y) (kN)	Yield displacement (Δ_y) (mm)	Horizontal ultimate load p_u (kN)	Angle of elastic-plasticity deflection (δ)	Coefficient of ductility (μ)
C02	257.8	16.527	298.8	1/32	3.2
Y01	258.9	14.578	304.53	1/34	3.6

maximum load point A is taken as the horizontal line AC, and then the oblique line OD is led by the origin O to cross the horizontal line AC at the point D, and the point D moves on the AC so that the area of the shaded part ① in the figure is equal to that of the shaded part ②. Then, point D is used as the vertical skeleton curve to point B, and point B is the obtained yield point.

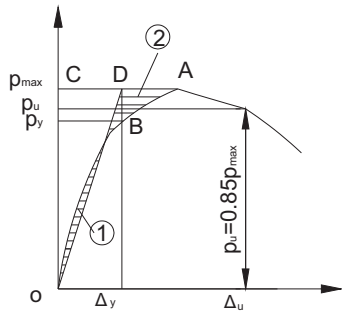

Fig. 11. The energy equivalent principle

The angle of elastic-plasticity deflection (δ) and coefficient of ductility (μ) are calculated as following equations:

$$\delta = \frac{\Delta_y}{H} \tag{4.1}$$

$$\mu = \frac{\Delta_u}{\Delta_y} \tag{4.2}$$

where H is the height from loading point to the column bottom.

It appears that the seismic performance parameters for C02 and Y01 are similar. The information in Table 3 can give a quantitative evaluation of the seismic performance of two specimens with the same reinforcement area ratios and axial compression ratio. So under high axial compression ratio, the cast-in-place column can be replaced by assembled monolithic column with SST+BB.

4.2.2. Specimen Y02 and C01

Fig. 12 shows the experimental responses of specimens Y02 and C01. All parameters pertaining to their anti-seismic capability are summarized in Table 4. The full load-displacement responses of Y02 and C01 under an axial compression ratio of 0.3 are shown in Fig. 12a, where the strength was developed and sustained as shown again by the backbone curves in Fig. 12b. Due to the same failure modes, the two specimens showed similar load–displacement behavior. Compared with Fig. 9 for columns Y01 and C02, it is clear that column specimens with low axial compression ratios showed different shapes of the load–displacement curve.

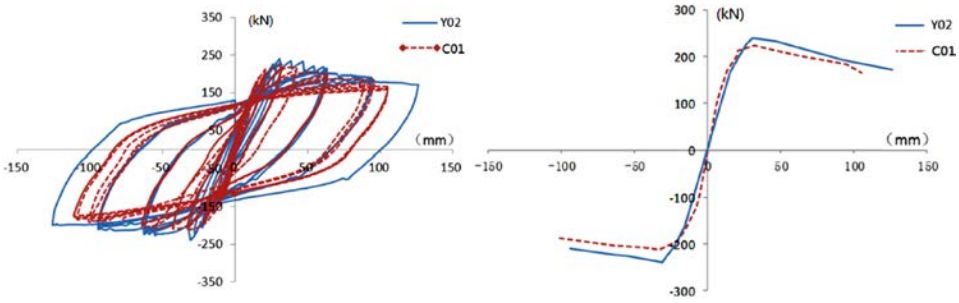

(a) (b)

Fig. 12. Load-displacement response of C01 and Y02: (a) hysteretic curve, (b) backbone curve

Table 4. Parameters of anti-seismic ability of Y02 and C01

Marks of the specimen	Yield load (P_y) (kN)	Yield displacement (Δ_y) (mm)	Horizontal ultimate load p_u (kN)	Angle of elastic-plasticity deflection(δ)	Coefficient of ductility (μ)
C01	187.1	20.1	218.9	1/16	5.3
Y02	215.2	20.0	239.4	1/14	6.0

Under an axial compression ratio of 0.3, the bearing capacity of the precast column (Y02) with SST + BB was similar to that of the cast-in-place column, but its angle of elastic–plastic deflection and ductility coefficient were significantly greater than those of the cast-in-place column. The overall performance of specimen Y02 was better than that of specimen C01. The influence of the SST + BB joint of the pre-cast columns was difficult to identify owing to limited data. However, the information in Table 4 can give a quantitative evaluation of the seismic performance of the assembled monolithic specimens and cast-in-place specimens.

5. Experimental results and discussion

5.1. Energy dissipation capacity

The energy dissipation capacity criterion is among the customary criteria for the estimation of the robustness of structural members against earthquakes. The hysteresis energy dissipation coefficient is calculated based on the normalization of the hysteretic dissipation energies of two equivalent triangular areas shown in Fig. 13 [22].

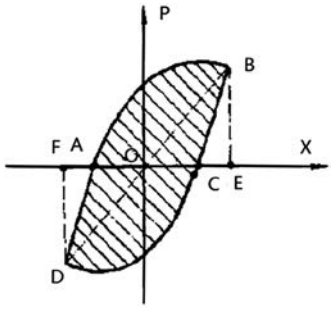

Fig. 13. Illustration of E

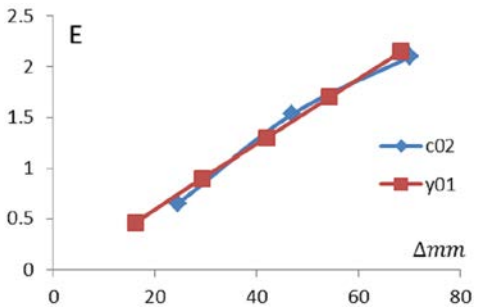

Fig. 14. Energy dissipation coefficient

In Fig. 14, the hysteresis energy dissipation coefficient of the specimens is shown with displacement. The coefficient shows the value of hysteresis energy dissipation in each cycle, which was normalized to the energy dissipation of an equivalent elastic cycle to provide a good criterion for a quantitative comparison of pinching. In general, the hysteresis energy dissipation coefficient increased with increasing drift (Fig. 14). The trends for specimens C02 and Y01 were very similar. The response of the assembled monolithic specimens in terms of energy dissipation was as satisfactory as that of the cast-in-place specimens.

$$E = \frac{S_{(\mathrm{ABC+CDA})}}{S_{(\mathrm{OBE+ODF})}} \tag{5.1}$$

5.2. Secant stiffness

The secant stiffness (K) calculated at each cycle of each successive displacement was used for a comparison of stiffness degradation among the test specimens. Secant stiffness is defined as the slope of a straight line between the maximum displacement levels of the given load cycle. The following formula was applied to calculate cyclic secant stiffness at different cycles. It was proposed by Ricles et al. [23]. Parameters for the calculation of cyclic stiffness are shown in Fig. 15.

$$K_i = \frac{|+F_i| + |-F_i|}{|+d_i| + |-d_i|} \tag{5.2}$$

The cyclic stiffness curves of the specimens are shown in Fig. 16. It is clear that the stiffness degradation of specimens C02 and Y01 were very similar, especially at higher

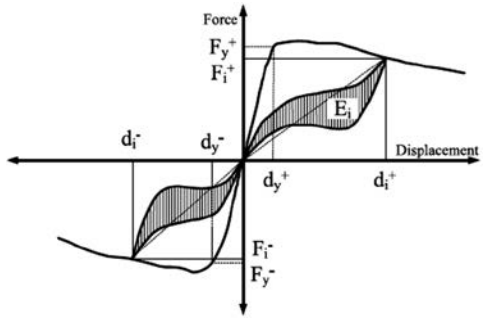

Fig. 15. Cyclic stiffness calculation parameters

drift levels. The loss of initial stiffness for these two columns was approximately 75–80% at the end of the previous cycle (Fig. 16). The stiffness of specimen Y01 was smaller than that of C02 for the third cycle of 30 mm drift because of the small slippage between the steel pipe and the concrete columns. However, the degradation in stiffness was slow at higher drift levels. The rough surface of the checkered steel plate was inward, which enhanced the cohesion between the surface of concrete and the steel plate.

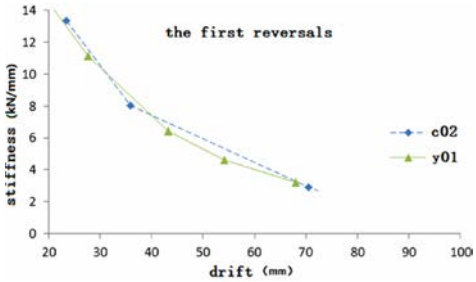

(a)

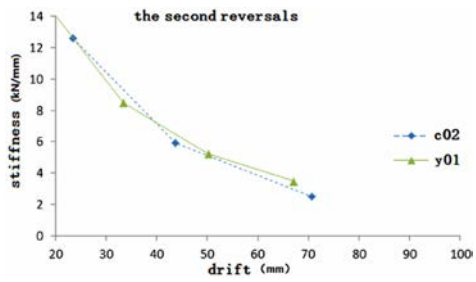

(b)

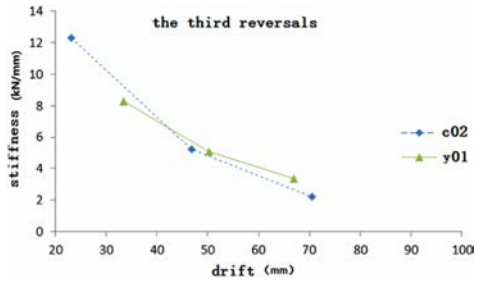

(c)

Fig. 16. The cyclic stiffness: (a) the first reversal, (b) the second reversal, (c) the third reversal

5.3. Node force transmission mechanism analysis

There was no slip between the concrete members and the local outsourced steel tube in the experiments. The connections can thus be seen as concrete-filled steel tube structures, and a crossing bolt bar for shear connection keys. The bonding force between steel tube and concrete helped prevent slip between the concrete members and the local outsourced steel tube. Thus, the load transfer of the concrete members with the steel tube (rod bolt connection) joints was as shown in Fig. 17. The moment-based resistance of the composite connection, M_u is given by

$$M_u = M_1 + M_2 \tag{5.3}$$

An empirical method of calculation based on the test results was used to predict he shear bonding capacity between concrete members and local outsourced steel tube. This was proposed by [24]:

$$\tau_u = 0.1 f_{cu}^{0.4} \tag{5.4}$$

where: τ_u (MPa) represents the shear bonding capacity as shown in Fig. 17 and f_{cu} (MPa) represents the compressive strength of concrete.

A method to predict the shear capacity of single-bolt reinforcement is proposed here. It assumes that:

$$V_s = A_{st} f_y / \sqrt{3} \tag{5.5}$$

where: V_s represents shear capacity as shown in Fig. 17, f_y represents the yield strength of the steel bar, and A_{st} represents the cross-section of single-bolt reinforcement.

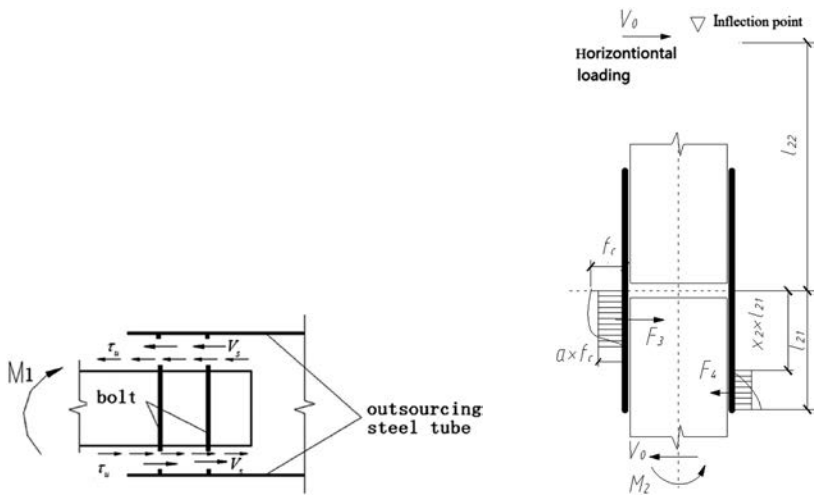

(a) (b)

Fig. 17. The force and the components of the composite joint

The moment-based resistance of the composite connection M_1 is given by:

$$M_1 = \left(V_u + \frac{1}{2}\tau_u l_n b_c\right) h_c \tag{5.6}$$

where: h_c is the depth of the concrete-assembled monolithic column; l_n is the length of the local outsourced steel tube; b_c is the thickness of the concrete column; τ_u is the shear capacity of the bolt reinforcements; and $V_u = n_1 V_s$, n_1 is the number of bolt reinforcements.

We assumed that the lateral compressive stress of the concrete columns was a rectangular distribution at connection failure. In Fig. 17b, the moment-based resistance of the composite connection M_2 is given by

$$M_2 = F_3\left(l_{21} - \frac{1}{2}x_2 l_{21}\right) - \frac{F_4}{2}(1 - x_2)\, l_{21} \tag{5.7}$$

The shear capacity of the composite connection V_0 is

$$V_0 = F_3 - F_4 \tag{5.8}$$

and:

$$M_2 = V_0\,(l_{21} + l_{22}) = F_3\left(l_{21} - \frac{1}{2}x_2 l_{21}\right) - \frac{F_4}{2}(1 - x_2)\, l_{21} \tag{5.9}$$

where l_{21} is half the length of the local outsourced steel tube; and l_{22} is the length of the local outsourced steel tube to the inflection point; and F_3, F_4 is the lateral compression of the concrete columns when $\alpha = 0.8$, then,

$$F_3 = 0.8 f_c x_2 l_{21} b_c \tag{5.10}$$

$$F_4 = 0.8 f_c (1 - x_2) l_{21} b_c \tag{5.11}$$

where f_c is the design value of concrete strength, such that:

$$x_2 = \frac{\sqrt{(l_{21} + 2l_{22})^2 + l_{21}^2} - 2l_{22}}{2l_{21}} \tag{5.12}$$

$$V_0 = 0.8 f_c \left(\sqrt{(l_{21} + 2l_{22})^2 + l_{21}^2} - (l_{21} + 2l_{22})\right) b_c \tag{5.13}$$

$$M_2 = V_0(l_{21} + l_{22}) = 0.8 f_c \left(\sqrt{(l_{21} + 2l_{22})^2 + l_{21}^2} - (l_{21} + 2l_{22})\right) b_c (l_{21} + l_{22}) \tag{5.14}$$

In this experiment, the steel bar was 22 mm in diameter, and single shear capacity of the steel bar was:

$$V_s = A_{st} f_y / \sqrt{3} = \frac{1}{4} \times 3.14 \times 22^2 \times 360/\sqrt{3} = 78.97 \text{ kN} \tag{5.15}$$

When $f_c = 29.27$ MPa, $l_c = 850$ mm, $n_1 = 4$, $b_c = 400$ mm, then:

$$M_1 = (4 \times 78970 + 0.5 \times 0.1 \times 29.27^{0.4} \times 850 \times 400) \times 400 = 152.60 \text{ kN} \cdot \text{m}$$

When $l_{22} = 1200 - 200 = 1000$ mm, $l_{21} = (850 - 50)/2 = 400$ mm, then:

$$M_2 = V_0(l_{21}+l_{22}) = 0.8 f_c \left(\sqrt{(l_{21}+2l_{22})^2 + l_{21}^2} - (l_{21}+2l_{22})\right) b_c(l_{21}+l_{22}) = 432.7 \text{ kN·m}$$

The comparison between the test results and those from the methods above is shown in Table 5. The results show that the moment capacity (585.32 kN·m) of the composite connections was larger than the test results for the specimen ($M_{tu} = V_{t0}(l_{21} + l_{22}) = 304.53 \times 1.4 = 426.342$ kN·m). So, damage was initiated at the bottom of each column, and thus an adequate moment capacity of the composite connection can be achieved.

Table 5. Comparison of test results and the proposed method for moment capacity of the composite connection

Marks of the specimen	Horizontal ultimate load V_{t0} (kN)	Test results M_{tu} (kN·m)	Calculated results M_1 (kN·m)	Calculated results M_2 (kN·m)	Calculated results M_{cu} (kN·m)
Y01	304.53	426.342	152.60	432.7	585.32
Y02	239.4	335.16	152.60	432.7	585.32

6. Conclusions

Based on the test results and observations made during the reverse cyclic test, the following conclusions can be drawn:

1. The failure modes of all columns are the large eccentric damage, and the destruction of all specimens occur at the column foot.
2. The hysteresis curves of the assembly column were plump with slight pinching. Both cast-in-place HSSS columns and the assembled monolithic HSSS columns under high axial pressure ratios exhibited good ductility. Under a uniform reinforcement ratio and axial compression ratio, the seismic performance of the prefabricated concrete columns with SST + BB joints was similar to that of the cast-in-place columns.
3. The trends of increase in the hysteresis energy dissipation coefficient with increasing drift of C02 and Y01 were very similar. The influence of the SST + BB joint of the precast columns was minor.
4. The degradation in the stiffness of specimens C02 and Y01 was very similar, indicating that the connections can be applied to seismic districts.
5. Comparisons of performance parameters, such as the yield load, ultimate load, coefficient of ductility, and energy dissipation capacity of the assembled monolithic HSSS columns with SST + BB were similar to or better than those of the cast-in-place columns. Thus, precast HSSS concrete columns may be suitable for use in earthquake zones.

Acknowledgements

This work was supported by the key scientific and technological research project of Science and Technology Department of Henan Province (Grant No. 222102320027) and Key R&D projects in Guangxi (Guike AB22036001, Guike AB21220046).

References

[1] L. Qingning, X. Zheng, Z. Yan, W. Jiang, and S. Pan, "Seismic behavior experimental study and theoretical analysis on high-strength continue compound spiral hoop confined concrete column", *Journal of Building Structures*, vol. 34, no. 8, pp. 90–99, 2013, doi: 10.14006/j.jzjgxb.2013.08.011.

[2] O.A. Taha, *Influence of diagonal reinforcement with spiral stirrups on shear capacity of coupling beam in shear wall*. M.A. Thesis, Faculty of Civil Engineering, Universiti Technologi Malaysia, 2013.

[3] M. Hadi, "Behaviour of high strength axially loaded concrete columns confined with helices", *Construction & Building Materials*, vol. 19, no. 2, pp. 135–140, 2005, doi: 10.1016/j.conbuildmat.2004.05.006.

[4] K.K. Arani, M.S. Marefat, A. Amrollahi-Biucky, et al., "Experimental seismic evaluation of old concrete columns reinforced by plain bars", *Structural Design of Tall & Special Buildings*, vol. 22, no. 3, pp. 267–290, 2013, doi: 10.1002/tal.686.

[5] H. Ding, L. Yuan, H. Chao, et al., "Seismic Performance of High-Strength Short Concrete Column with High-Strength Stirrups Constraints", *Transactions of Tianjin University*, vol. 23, no. 4, pp. 360–369, 2017, https://kns.cnki.net/KCMS/detail/detail.aspx?dbcode=CJFD&filename=TJDY201704007.

[6] J. Qinjian, "Summary on development of assembled concrete building both home and abroad", *Journal of Architecture Technology*, vol. 41, no. 12, pp. 1074–1077, 2010, doi: 10.3969/j.issn.1000-4726.2010.12.001.

[7] L.I. Jin, et al., "Test research on seismic performance of new-type assembled monolithic short columns", *World Earthquake Engineering*, vol. 30, no. 1, pp. 29–33, 2014.

[8] X.H. Zhang, et al., "Experimental research on seismic performance of new fabricated column spliced by grout sleeves", *Journal of Xi'an University of Architecture & Technology*, vol. 45, no. 2, pp. 63–73, 164–170, 2013, doi: 10.15986/j.1006-7930.2012.03.018.

[9] J. Chen and Y. Xiao, "Experimental study on seismic behavior of precast concrete column with longitudinal reinforcement grouting-anchoring connections", *China Civil Engineering Journal,* vol. 49, no. 5, pp. 63–73, 2016, doi: 10.1177/1369433219858451.

[10] Ch.L. Wang, et al., "Seismic performance of slurry anchor lapping of corrugated pipe restrained by spiral stirrup", *Industrial Construction,* vol. 51, no. 4, pp. 126–131, 2021, doi: 10.13204/j.gyjzg19110704.

[11] M. Wang, S.T. Liang, and K.L. Li, "Experimental study of new total-prefabricated concrete frame column with dry-connection under low reverse cyclic loading", *Architecture Technology*, vol. 41, no. 1, pp. 52–55, 2010, doi: 10.3969/j.issn.1000-4726.2010.01.016.

[12] T. Ozturan, S. Ozden, and O. Ertas, "Ductile Connections in Precast Concrete Moment Resisting Frames", *Prestressed Concrete Institute Journa*l, vol. 51, pp. 66–76, 2006, doi: 10.15554/pcij.05012006.66.76.

[13] Y.C. Loo and B.Z. Yao, "Static and repeated load test on precast concrete beam-to-column connections", *Journal of Precast/Pre-stressed Concrete Institute*, vol. 40, no. 2, pp. 106–115, 1995, doi: 10.15554/pcij.03011995.106.115.

[14] GB50010-2010 Chinese National Standards, Code for Design of Concrete Structures. Architecture and Building Press, Beijing, 2015.

[15] GB 50367-2006 Chinese National Standards, Code for Concrete Reinforcement Design. Architecture and Building Press, Beijing, 2006.

[16] GB 50017-2017 Chinese National Standards, Code for Design of Steel Structures. Architecture and Building Press, Beijing, 2017.

[17] L. Xiong, H. Chen, Z. Xu, et al., "Experimental study on shear mechanical properties of through-step joints under direct shear", *Archives of Civil Engineering*, vol. 68, no. 4, pp. 45–61, 2022, doi: 10.24425/ace.2022.143025.

[18] W.P. Cheng, Y.P. Song, and J. Wang, "Expermental study of seismic performance for beamŻcolumn joints of precast and discontinuous steel reinforced concrete frames", *Dalian Ligong Daxue Xuebao/Journal of Dalian University of Technology*, vol. 55, no. 2, pp. 171–178, 2015, doi: 10.7511/dllgxb201502008.

[19] M. Szadkowska and E. Szmigiera, "Bond Between Steel and Self-Compacting Concrete in Composite Tube Columns", *Archives of Civil Engineering*, vol. 63, no. 2, pp. 131–143, 2017, doi: 10.1515/ace-2017-0021.

[20] S. Bousias, A.L. Spathis, and M.N. Fardis, "Seismic retrofi tting of columns with lap spliced smooth bars through FRP or concrete jackets", *Journal of Earthquake Engineering*, vol. 11, no. 5, pp. 653–674, 2007, doi: 10.1080/13632460601125714.

[21] C. Christopoulos, A. Filiatrault, C.M. Uang, and B. Folz, "Post-tensioned energy dissipating connections for moment-resisting steel frames", *Journal of Structural Engineering*, vol. 128, no. 9, pp. 1111–1120, 2002, doi: 10.1061/(ASCE)0733-9445(2002)128:9(1111).

[22] P. Rojas, J.M. Ricles, and R. Sause, "Seismic Performance of Post-tensioned Steel Moment Resisting Frames With Friction Devices", *Journal of Structural Engineering*, vol. 131, no. 4, pp. 529–540, 2015, doi: 10.1061/(ASCE)0733-9445(2005)131:4(529).

[23] J.M. Ricles, R. Sause, S. Pessiki, and L.W. Lu, "Experimental evaluation of earthquake resistant post-tensioned steel connections", *Journal of Structural Engineering*, vol. 128, no. 7, pp. 850–859, 2002, doi: 10.1061/(ASCE)0733-9445(2002)128:7(850).

[24] U. Ersoy and T. Tankut, "Precast Concrete Members With Welded Plate Connections Under Reversed Cyclic Loading", *Prestressed Concrete Institute Journa*l, vol. 38, no. 4, pp. 94–100, 1993, doi: 10.15554/pcij.07011993.94.100.

Received: 2023-02-16, Revised: 2023-06-13